VNU Journal of Science: Mathematics - Physics

Journal homepage: https://js.vnu.edu.vn/MaP

Original Article

Study on the Palladium Nucleation and Growth Mechanism in A Deep Eutectic Solvent by Electrochemical Method

Dao Vu Phuong Thao[1], Dang Thi Thuy Ngan[1], Dinh Van Tuan[2], Hoang Lan[1], Nguyen Thi Nguyet[3], Nguyen Dac Dien[4], Vu Van Thu[4], Pham Hung Vuong[5], Phuong Dinh Tam[1,*]

[1]*Phenikaa University, Nguyen Trac, Ha Dong, Hanoi, Vietnam*

[2]*Electric Power University, 235 Hoang Quoc Viet, Cau Giay, Hanoi, Vietnam*

[3]*Hung Yen University of Technology and Education, Yen Lich, Dan Tien, Khoai Chau, Hung Yen, Vietnam*

[4]*Vietnam Trade Union University, 169 Tay Son, Dong Da, Hanoi, Vietnam*

[5]*International Training Institute for Materials Science, Hanoi University of Science and Technology, 1 Dai Co Viet, Hai Ba Trung, Hanoi, Vietnam*

Received 05 July 2023
Revised 29 August 2023; Accepted 18 March 2024

Abstract: By using cyclic voltammetry (CV) and chronoamperometry (CA) techniques, the thermodynamics and kinetics of palladium electrodeposition on glassy carbon electrode (GCE) in deep eutectic solvent were studied. The Pd electrodeposition process via progressive 3D nucleation mechanism was controlled by the diffusion. Non-linear fitting methods were applied to obtain the kinetic parameters in the light of Harrison – Thirsk (H-T) and Scharifker – Hills (S-H) models for 3D nucleation and growth process. From that, the diffusion coefficient of Pd (II) in reline at ambient temperature was calculated by two different ways, and the obtained results showed that it is of 1.612×10^{-8} cm^2/s by using CV. Moreover, some important parameters such as the number density of active sites on the electrode surface (N_o) and the nucleation frequency per active site (A) were estimated by fitting experimental CAs data with Scharifker-Mostany model.

Keyword: Electrodeposition, thermodynamic, electrochemical, progressive, palladium, deep eutectic solvent.

* Corresponding author.
E-mail address: tam.phuongdinh@phenikaa-uni.edu.vn

https//doi.org/10.25073/2588-1124/vnumap.4861

1. Introduction

Electrochemistry is a powerful technique to probe reactions involving electron transfers [1] which results in the oxidation or reduction of a metal complex. In an electrochemical reduction, a metal ion is reduced via heterogeneous electron transfer from an electrode. Through use of a potentiostat, voltage is applied to the electrode to modulate the energy of the electrons in the electrode. When the energy of electrons in the electrode is larger than the lowest unoccupied molecular orbital (LUMO) of metal ions, an electron from the electrode is transferred to metal ion. The difference in energy levels between the electrode and the LUMO of metal ion is the driving force for the electrochemical reaction. The driving force of a reaction can be controlled and the thermodynamic and kinetic parameters can be measured [1]. A great deal of interest in modern electrochemistry has been intended for the metal electrocrystallization on various substrates [2-4]. The physico-chemical properties of electrodeposits are determined by the nucleation kinetics and the growth of metallic nuclei on the substrate [5].

Palladium (Pd) is one of the most attractive metals because it has many excellent physical and chemical characteristics such as high catalytic activity, corrosion and wear resistance, thermal stability and biocompatibility properties [4, 6, 7]. Therefore, Pd and its compounds are used for many industrial applications, especially in catalytic and electrical devices such as hydrogenation catalysts [8], solar cell [9], oxidation of benzyl alcohol [10], ethanol oxidation [11], biosensors [12-14]. Pd has been electrodeposited on various electrodes containing polymer matrix, porous stainless steel electrode, copper and gold single crystal electrode, graphite substrate [15-17]. Electrodeposition of Pd and cobalt on glassy carbon electrode has received some attention by several authors [3, 4, 18].

In terms of synthesizing Pd nanoparticles, electrochemical techniques are used widely due to its convenience, simplicity and low-cost [2, 19-21]. Recently, ionic liquid solvents and deep eutectic solvents are studied to use for electrodeposition of metals due to their special properties such as thermal stability, non-hydrogen liberation and wide electrochemical window [3, 22, 23]. Yoshii et al., studied the electrodeposition of palladium from palladium (II) acetylacetonate in an amide-type ionic liquid at the ambient temperature with the average size of 2.8 nm [19]. Lanzinger et al., compared the electrodeposition of palladium in different solvents including choline chloride (ChCl)-urea, ChCl-ethylene glycol and 1-butyl-3-methylimidazolium chloride-tetrafluoroborate solution. They found that palladium deposits from the ChCl-urea solvent are fine-grained, with no cracks [20]. Juarez-Marmolejo et al., synthesized palladium nanoparticles using $PdCl_2$ dissolved in ChCl-urea solvent by electrochemical method. They found that metallic palladium nanoparticless (Pd NPs) were dispersed homogeneously on the GCE substrate with a mean size of around 60 nm [2]. M. Manolova et al. studied the influence of additives and electroplating parameters on the morphology of Pd NPs using palladium (II) chloride dissolved in ChCl/urea solvent [21].

In addition, studying on electro-mechanism plays an important role in the understanding about nucleation and growth of metal. Danaee studied the Pd nucleation and growth mechanism on graphite electrode using $Pd(NH_3)_4Cl_2$ solution , NH_4Cl, and NH_4OH by means of electrochemical method at room temperature. It was reported that the initial stage occurred instantaneous two-dimensional nucleation and growth and then a multitude of progressive steps followed the double layer charging [7]. Fuentes et al. investigated that mechanisms of Pd electrodeposition on two different electrodes (highly oriented pyrolytic graphite and titanium) in $PdCl_2$ and HCl solution were 3D instantaneous nucleation and growth controlled by diffusion [24]. Espino-Lopez et al., found that the formation of Pd NPs onto GCE in ChCl-ethylene glycol solvent at 298 K follows the 3D nucleation with controlled by diffusion-controlled growth. The Pd NPs were uniformly distributed onto the electrode surface, with particle size of about 45 nm [18]. Aguirre studied the electrodeposition of Pd in a solution of K_2PdCl_4 and HCl. The author

showed that the metallic Pd formation on Ti electrode occurred via at least three processes: adsorption, 2D nucleation with adsorption-atoms incorporation-controlled growth, and 3D nucleation with diffusion-controlled growth, while that on GCE follows 3D instantaneous nucleation and diffusion-controlled growth [25].

However, there is still a shortage of the knowledge about the first stage of Pd electrodeposition in reline at room temperature. Some kinetic parameters such as the nucleation frequency, A, the number density of active sites for Pd nucleation onto the electrode surface, N_o, have not been reported. Therefore, this work aims to investigate the mechanism of Pd nucleation and growth onto glassy carbon electrode from ChCl/urea/palladium mixture at room temperature using cyclic voltammetry (CV) and chronoamperometry (CA) techniques. Furthermore, X-ray diffraction, scanning electron microscopy and energy dispersive X-ray spectroscopy were used to examine the crystalline structure, morphology and compositions of deposited Pd samples.

2. Experimental Methods

2.1. Chemical Reagents

Choline chloride ($C_5H_{14}ClNO$, 98%), urea (NH_2CONH_2, 98%), palladium (II) chloride ($PdCl_2$, 99%) were purchased from Sigma Aldrich.

2.2. Electrolyte Preparation from A Mixture Choline

Reline was synthesized by stirring the mixture in a 1/2 molar ratio of choline chloride with urea at 100 °C until obtaining transparent homogenous liquids. Then, palladium (II) chloride salt was added to this liquid under continuously stirring for 12 hours to acquire 50 mM Pd (II) solution. This solution was used in later measurements.

2.3. Electrochemical Measurement

The vessel used for a cyclic voltammetry experiment is called an electrochemical cell. Figure 1 presents a schematic representation of an electrochemical cell used for CV and CA tests. Three-electrode setup includes a 0.0707 cm^2 area glassy carbon electrode (GCE) as working electrode (WE), platinum wire counter electrode (CE), and Ag/AgCl reference electrode (RE). The CE is chosen to be as inert as possible and is isolated from the rest of the system by a fritted compartment. CA and CV measurements were carried out using VersaStat 3 system, coupled to the VersaStudio software installed in a PC for experimental control and data collection. These experiments were performed at room temperature. The cyclic voltammetry can provide useful information for the electron transfer reactions as well as kinetic and mechanistic of chemical reactions [26].

Ions migrate in solution to maintain the electrical neutrality as the electrons transfer from the electrode to the analyte. A supporting electrolyte, for instance, a salt, is dissolved in the solvent to form an electrolyte solution to help decrease the solution resistance. Reline is a good solvent because it can dissolve the analyte and supporting electrolyte completely, not oxidized or reduced in the potential range of the experiment, not lead to deleterious reactions with the analyte or supporting electrolyte. A good supporting electrolyte is chemically and electrochemically inert in the conditions of the experiment and increase solution conductivity. It will migrate to balance the charge and complete the electrical circuit as the electron transfers occur at the electrodes. Without supporting electrolyte, the solution resistance will increase and the charge transfer will decrease. The concentration of the dissolved salt affects the

conductivity of the solution. Ionic solute moves by action of an electric field, positive ions are attracted to negative electrodes. The difference in concentration in the electrochemical cell leads to diffusion of analyte from areas of high to low concentration. The electrolyte will migrate to the electrode surface for charge balance.

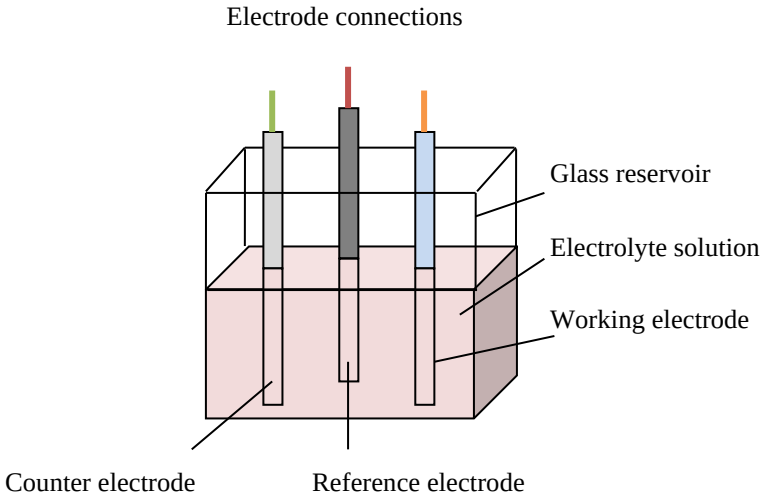

Figure 1. Schematic representation of how to assemble an electrochemical cell to collect data during CV experiments [7].

The analyte was added into the assembled cell, then an open circuit potential (OCP) develops at the electrodes to equilibrate with the solution so that no current flows. The OCP gives information about the redox state and the concentration of species in the solution. To mitigate the Ohmic drop phenomenon, we should reduce the size of the working electrode, restrict the experiment to slow scan rates, increase the conductivity of the solution with higher electrolyte concentrations, and diminish the distance separating the reference and working electrode [27]. The electrode reaction involves the charge transfer between an electrode and a species in solution. In which, reactant moves to the interface, electron transfer occurs between the electrode and reactant, and the product moves away from the electrode to allow fresh reactant to the surface. By keeping track of the number of electrons flowing (through measuring the current or current density), we can say the number of metal ions have been reduced.

The cyclic voltammograms (CV) were recorded in the potentials between -0.8 V and 1 V (interval of 50 mV) for a solution of Pd (II) (50 mM in reline) with the scan rate of 50 mV/s at room temperature. To study the influence of various scan rates (v) on the CV responses, v was controlled from 10 to 100 mV/s. The amperometric measurements were performed in the applied potential range from -0.51 V to -0.56 V.

2.4. Characterization

The size and shape of Pd NPs synthesized by electrochemical method was characterized by a FESEM HITACHI S-4800 which combines EDS technique for analysis of compositions. X-ray diffraction pattern of the palladium electrodeposited on GCE was got through an Empyrean X-ray diffractometer using the monochromatic Cu-K_α radiation with a wavelength of 1.5406 Å.

3. Results and Discussion

3.1. Characterization

The Pd surface morphology on GCE in reline was studied by means of FESEM. Pd NPs obtained in reline solution were shown in Figure 2a with a different sizes and distributions (Figure 2b). To be more specific, the size of particles was in the range from 10 nm to nearly 250 nm. Besides, the number of particles having the size of around 70-80 nm were highest. This demonstrated that the Pd nucleation was followed the progressive mechanism.

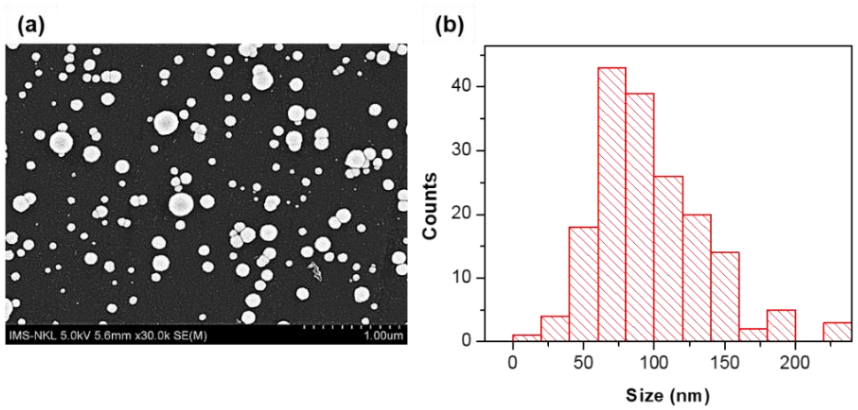

Figure 2. a) SEM image of Pd NPs deposited on GCE obtained in reline (-0.43 V in 40 s): b) Distribution of Pd NPs sizes determined from the SEM image.

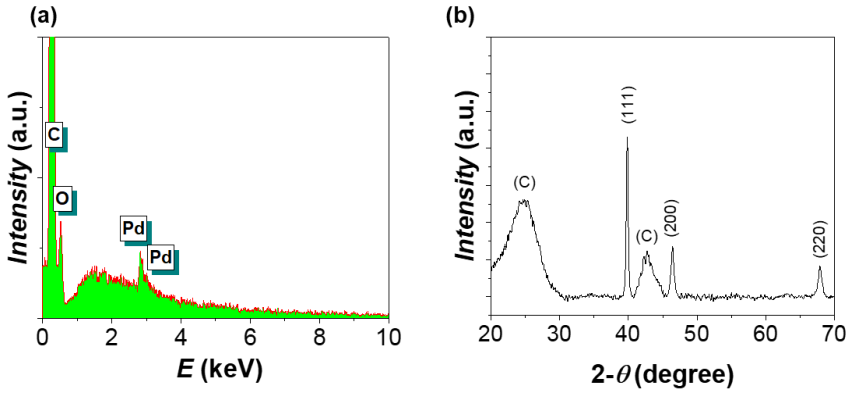

Figure 3. a) EDS spectrum; b) XRD pattern of Pd NPs deposited on GCE.

The EDS spectrum of Pd sample deposited on GCE in reline at -0.43 V in 40 s was also illustrated in Figure 3a. According to the appearance of Pd peaks, it can be confirmed that Pd NPs were generated on the electrodes. Additionally, the presence of the carbon peak resulted from the electrode. The oxygen peak can be supposed to the oxidation of the outer layer of Pd. In addition, the crystalline structure of Pd on GCE in reline containing Pd (II) was confirmed through X-ray diffraction pattern (Figure 3b). Apart from the reflection peaks of carbon and Pd, in the XRD patterns there are no peaks of any impurities, this emphasized a high purity of the deposited samples. The peaks located at 2θ values of 39.85°, 46.4° and 67.96° corresponding to (111), (200) and (220) crystalline planes, respectively, as indicated by the face-centered cubic (FCC) lattice of Pd.

3.2. CV Characterization

Cyclic voltammetry (CV) is employed commonly to investigate the reduction and oxidation processes of molecular species and to study electron transfer-initiated chemical reactions. The x-axis represents the applied potential (E), while the y-axis is the resulting current density (j). The arrow indicates the direction in which the potential was scanned to record the data, and the caption indicates the condition of the experiment. In the forward scan, the potential is swept negatively from the starting potential E_1 to the switching potential E_2 to form the cathodic trace. Then, the scan direction is reversed, and the potential is swept positively back to E_1 to generate the anodic trace [28]. When $PdCl_2$ solution is scanned to negative potentials, Pd^{2+} is reduced to Pd locally at the electrode, resulting in the depletion of Pd^{2+} at the electrode surface, and the concentration of Pd at the electrode surface increases. The current is dictated by the delivery of additional Pd^{2+} via diffusion from the bulk solution and the diffusion layer at the surface of the electrode containing the reduced Pd continues to grow throughout the scan. When the scan direction is reversed, the potential is scanned in the positive (anodic) direction. The Pd present at the electrode surface is oxidized back to Pd^{2+} as the applied potential becomes more positive (Figure 4). The oxidation peak and reduction peak are separated due to the diffusion of the analyte to and from the electrode.

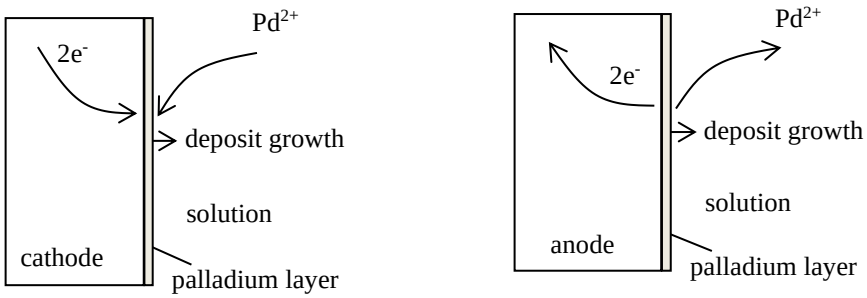

Figure 4. Reduction and oxidation reactions of Pd at working electrode.

Figure 5 shows the cyclic voltammogram (CV) conducted in reline containing 50 mM Pd (II) obtained in the potential range of -0.8 V to 1 V versus Ag/AgCl with the scan rate v = 50 mV/s at room temperature. According to this CV, the presence of nucleation loop which is considered as a typical characteristic of nucleation and growth is found in. Besides, it contains one reduction peak and one oxidation peak in two opposite scan directions. On the forward direction scan, there is one cathodic/reduction peak related to metallic formation process following the reaction:

$$Pd^{2+} + 2e \rightarrow Pd \quad (1)$$

The reduction peak is observed at -0.58 V and at more negative potential, current density increases further due to the hydrogen evolution. Meanwhile, the reverse scan shows initially a decrease in current density and two crossovers, one at -0.48 V and one at 0 V. The crossover loop signified nucleation in the course of the anodic scan [29]. One anodic/oxidation peak involving to oxidation process from metallic Pd to Pd (II) ions at 0.6 V associates with the reaction:

$$Pd - 2e \rightarrow Pd^{2+} \quad (2)$$

Furthermore, based on Figure 5, the equilibrium potential of the Pd (II)/Pd couple could be estimated as -0.4 V. Metal already deposited on the electrode surface continues to grow as a result of the reaction

(2). The nuclei growth rate is controlled by charge transfer and is determined only by the imposed potential [7].

To investigate the Pd electrochemical behavior on GCE in reline, a variety of CV having distinct scan rates (v) in the range from 10 mV/s to 100 mV/s was carried out (Figure 6a). During the experiment, the potential was varied linearly at the scan rate of v (mV/s). At larger scan rate, the diffusion is faster which means the diffusion layer decreases [27]. The results in the higher values of the peak current density (j_{cp}) when the scan rate is raised from 10 mV/s to 100 mV/s suggests that the activation-free energy at the peak is smaller, and the cathodic peak becomes more negative when raising the scan rate [27].

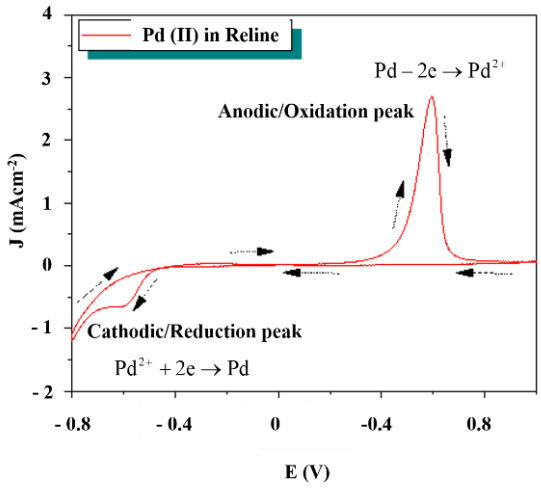

Figure 5. Cyclic voltammogram obtained onto GCE from the reline with 50 mM Pd (II) at scan rate of 50 mV/s at 25 °C.

For electrochemically reversible electron transfer process involving freely diffusing redox species, the dependence of the peak current on scan rate reveals the linear plot of j_{cp} versus $v^{1/2}$. Deviations from linearity in plot of j_{cp} versus $v^{1/2}$ suggest either electrochemical quasi-reversibility or the electron transfer via surface-adsorbed species [30].

Additionally, higher values of the peak current density (j_{cp}) are obtained at larger scan rates (v) owing to the decreasing of the diffusion layer [1]. In detail, j_{cp} and $v^{1/2}$ perform the linear dependence which suggests that the Pd formation on GCE in reline also emerge through a 3D diffusion-controlled process according to Berzins – Delahay model [3]:

$$j_{cp} = \frac{0.61(Fn)^{3/2} C_o (Dv)^{1/2}}{(RT)^{1/2}} \quad (3)$$

where F is Faraday's constant, R is the universal gas constant, n is the number of electrons transferred in the redox event, v is the scan rate (V/s), C_o is the bulk concentration of reduced species (mol/cm^3), D is the diffusion coefficient of Pd (II) ions (cm^2/s) and T is the temperature of medium (K).

The CV plots were used to investigate the formation of Pd NPs from DES (reline) onto GCE at different scan rates (10 – 100 mV/s) at room temperature. Figure 6b illustrates the cathode peak current density (j_{cp}) that depends on the scan rate (v). The result shows the linear dependence of j_{cp} on the square root of v ($v^{1/2}$) which is described by the following equation:

$$-j_{cp}\left(\frac{A}{cm^2}\right)=0.0034v^{1/2}\left(\frac{V^{1/2}}{s^{1/2}}\right)-0.0001\left(R^2=0.9988\right) \quad (4)$$

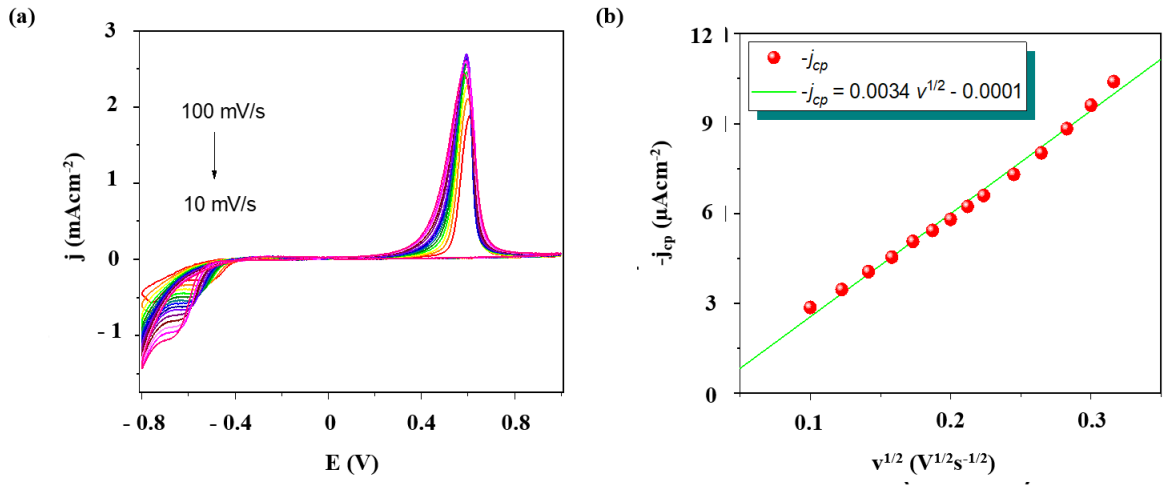

Figure 6. (a) CVs obtained on GCE in reline dissolving 50 mM Pd (II) with different scan rates, (b) linear dependence between j_{cp} and $v^{1/2}$.

The diffusion coefficients of Pd (II) ions in reline at room temperature were measured as $D=1.612\times10^{-8}\ cm^2/s$. In several previous publications, the diffusion coefficients of Pd (II) in reline and ethaline were estimated by means of cyclic voltammetry. For examples, Espino-Lopez et al., have measured the Pd (II) ions diffusion coefficient (D) in DES based on choline chloride and ethylene glycol at 298 K to be $D=2.77\times10^{-7}\ cm^2/s$ [18]. Lanzinger et al. have calculated the diffusion coefficient for Pd (II) in ChCl-urea solution at high temperature (50-100 °C) to be $D=1.7\ \text{to}\ 7.5\times10^{-8}\ cm^2/s$ [20]. The value of diffusion coefficient which we measured is smaller than others. This can be explained due to the lower temperature of our work leading to the lower diffusion coefficient.

3.3. CA Characterization

Chronoamperometry (CA) was used to examine the nucleation and growth mechanism of Pd in both reline and ethaline. The applied potential ranges for CA experiments were chosen from CV in Figure 5, from -0.51 V to -0.56 V. The obtained form of CAs was shown in Figure 7. These CAs have the same shape with which contains two stages. In the first stage, there is the increment of current density which is supposed to nucleation and growth of new phase. Here, the current density reaches its maximum (j_m) at a time t_m. In the next stage, the current density decays and becomes stable at longer time inasmuch as the increase and overlap of diffusion layer thickness of the growing nuclei according to Cottrell equation [31]. The value j_m increments and t_m tends to minimize at the more negative applied potential which can be explained due to the gradual increase of nucleation rate and nucleation density when the applied potentials shift negatively.

As can be seen in Figure 8, it is clear that there are two types of nucleation mechanism (progressive and instantaneous) with two kinds of growth mechanism (2D and 3D). Instantaneous nucleation means that the number of nuclei are generated promptly at a fast rate after applying the potential and keep unchanging over time; during the electrodeposition process, they continue to grow on these positions

and do not form any new nuclei [5, 32]. Thus, the sizes of nuclei particles are uniform. For the progressive nucleation, the nuclei not only grow on the previously formed positions but also on later creation nuclei at a slow rate, which leads the difference of the radii of the particles on the surface [5, 31]. In the 3D growth, the nuclei in the parallel or perpendicular directions grow equivalently. Meanwhile, in the 2D growth, the growth rate of nuclei in the parallel direction are larger than in the perpendicular direction [32].

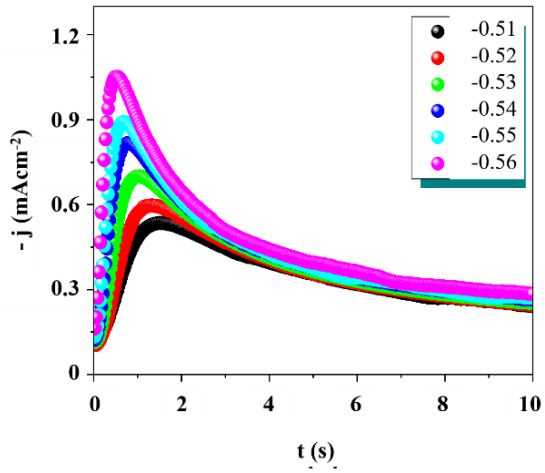

Figure 7. Current-time transients of the CA experiment performed on GCE in reline containing 50 mM Pd (II) at room temperature.

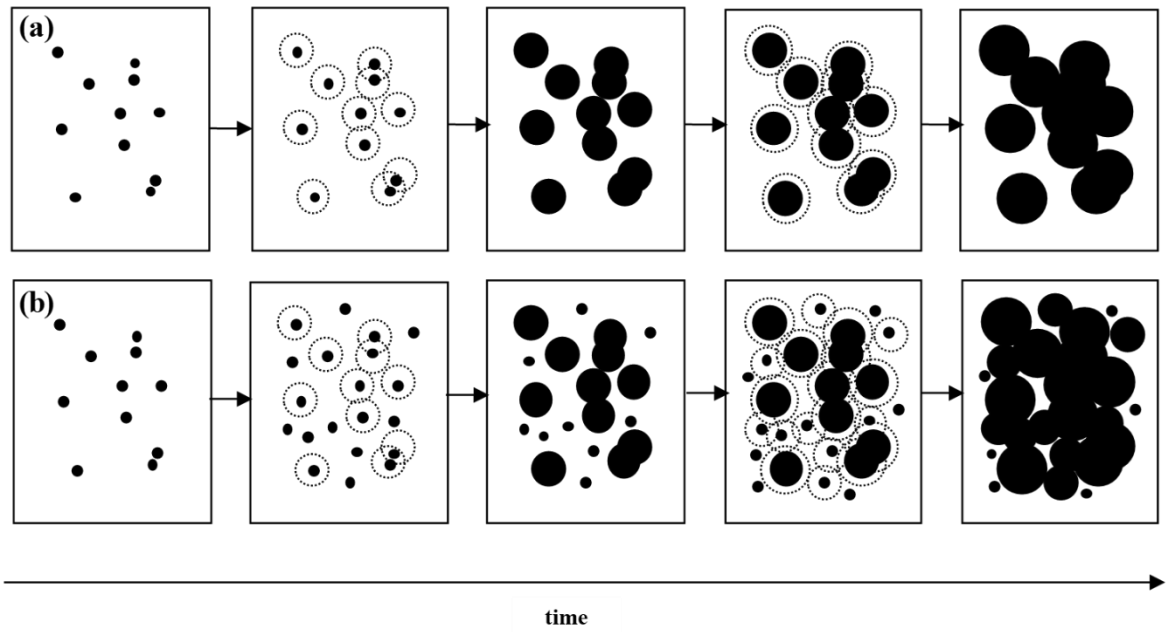

Figure 8. Illustration of two kinds of nucleation and growth mechanism: (a) instantaneous, (b) progressive.

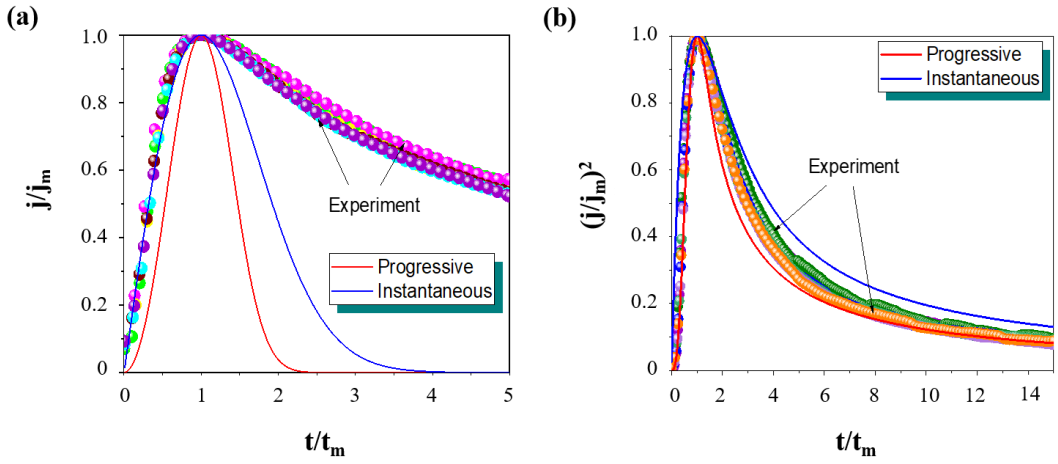

Figure 9. Comparison between theoretical nucleation curves of (a) Harrison – Thirsk model and (b) Scharifker – Hills model with the normalized plots of experimental current density transients obtained on GCE in reline.

In order to fully understand the mechanism of Pd electronucleation and growth, we use the Harrison – Thirsk (H-T) and Scharifker – Hills (S-H) models for 2D and 3D growth mechanism to investigate the experimental CAs. The non-dimensional curves from the obtained CAs were compared with the instantaneous and progressive plots of H-T model (Eqs. 5 – 6) and S-H model (Eqs. 7 – 8) (Figure 9), respectively [33]:

$$\frac{j}{j_m} = \left(\frac{t}{t_m}\right)^2 \exp\left\{\frac{2}{3}\left[1-\left(\frac{t}{t_m}\right)^3\right]\right\} \tag{5}$$

$$\frac{j}{j_m} = \frac{t}{t_m}\exp\left\{\frac{1}{2}\left[1-\left(\frac{t}{t_m}\right)^2\right]\right\} \tag{6}$$

$$\left(\frac{j}{j_m}\right)^2 = 1.9542\left(\frac{t}{t_m}\right)^{-1}\left\{1-\exp\left[-1.2564\frac{t}{t_m}\right]\right\}^2 \tag{7}$$

$$\left(\frac{j}{j_m}\right)^2 = 1.2254\left(\frac{t}{t_m}\right)^{-1}\left\{1-\exp\left[-2.3367\left(\frac{t}{t_m}\right)^2\right]\right\}^2 \tag{8}$$

As can be seen from Figure 9a upon examination of H-T model case, all experimental CAs lie out of the valid range formed by two theoretical plots. Therefore, the Pd electrodeposition is not followed the 2D nucleation and growth. In the S-H model case, as shown in Figure 9b, comparing the shape of these curves, the experimental plots are sited in the region supposed to be the 3D nucleation and growth which is restricted by instantaneous and progressive plots of the S-H model. In particular, the experimental normalized curves tend to approach the progressive curve that means the electronucleation of Pd in reline follows dominantly progressive nucleation mechanism. Pd electrodeposition in the choline chloride-urea at glassy carbon electrodes at 60 °C has been previously studied by Fousseni Soma et al., [4]. They found that the Pd electronucleation and growth follows the progressive mechanism which is same to our study instead of the difference of temperature.

Because the location of non-dimensional plots of experimental CAs are in the region of the 3D nucleation and growth, Scharifker – Mostany (SM) model can be used to represent the processes occurring onto GCE surface during the Pd electrodeposition and provide several typical parameters. The form of SM model with the 3D nucleation and growth is given by [3, 22]:

$$j(t)_{3D} = \frac{zFD^{1/2}C_o}{\pi^{1/2}t^{1/2}}\left\{1-\exp\left[-N_o\pi D\left(\frac{8\pi MC_o}{\rho}\right)^{1/2}\left(1-\frac{1-e^{-At}}{A}\right)\right]\right\} \quad (9)$$

where ρ is the density of the Pd deposit and M is the atomic mass, N_o is the number density of active sites on the electrode surface, and A is the nucleation frequency per active site (s^{-1}). zF is the molar charge transferred during the electrodeposition.

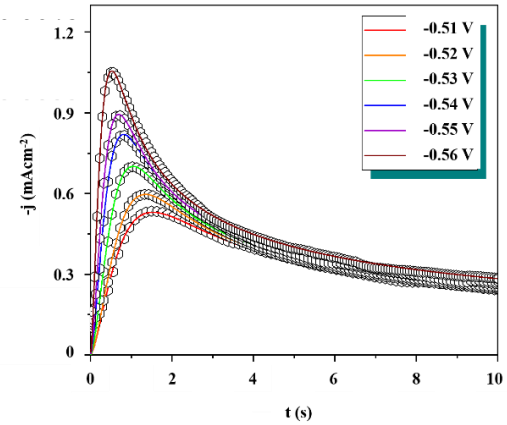

Figure 10. Comparison between the j-t transients and theoretical curves.

Table 1. The typical kinetic parameters revealed from Equation 9 in reline

E (V)	***A*** (s^{-1})	N_0 (10^{-7}) (cm^{-2})	***D*** (10^{-8}) ($cm^2\ s^{-1}$)	AN_0 (10^{-7}) ($cm^{-2}\ s^{-1}$)
-0.41	1.0155	3.0082	9.9872	3.0549
-0.42	1.4015	4.0251	9.1239	5.6413
-0.43	1.0280	6.4862	9.1766	6.6674
-0.44	1.2388	6.7830	9.2248	8.4028
-0.45	0.9236	10.6349	9.3130	9.8225
-0.46	1.3095	9.9483	9.3331	13.0273

Figure 10 presents a theoretically derived current transient at -0.51 and -0.56 V versus Ag/AgCl that agrees well with the experimental CAs using Eq. (9). Table 1 shows some typical parameters measured from fitting the CA curves. It is obviously realized that the values of AN_o product increase with the rise of the value of applied potential which confirmed the appreciation of the used model [3, 22].

4. Conclusion

The kinetics and mechanism of Pd electro-nucleation and growth on GCE from 50 mM $PdCl_2$, NH_2CONH_2, and $C_5H_{14}ClNO$ were clearly investigated by means of CV and CA methods in deep

eutectic solvent. The results revealed that electrodeposition of Pd in reline proceeds via nucleation and growth mechanism. Potential transient indicates that Pd reduction was controlled by the diffusion. From that, diffusion coefficient of Pd (II) ions in reline at ambient temperature was calculated. Furthermore, the CA results showed the significant effect of solvent on the Pd electrodeposition mechanism. More specific, it was followed dominantly progressive 3D nucleation mechanism. The classical SM model was able to use to examine kinetic parameters such as D, A and N_o, which AN_o product witnessed an exponential growth with applied potential.

Acknowledgements

This research was financially supported by Vietnam National Foundation for Science and Technology Development (NAFOSTED) under grant number 103.02-2019.337.

References

[1] N. Elgrishi, K. J. Rountree, B. D. McCarthy, E. S. Rountree, T. T. Eisenhart, J. L. Dempsey, A Practical Beginner's Guide to Cyclic Voltammetry, Journal of Chemical Education, Vol. 95, 2018, pp. m197-206, http://dx.doi.org/10.1021/acs.jchemed.7b00361.

[2] L. J. Marmolejo, B. M. Teodocio, M. G. M. D. O. Yemha, M. R. Romo, E. M. A. Estrada, A. E. Mejía, M.T. R. Silva, J. Mostany, M. P. Pardavé, Electrocatalytic Oxidation of Formic Acid by Palladium Nanoparticles Electrochemically Synthesized from a Deep Eutectic Solvent, Catalysis Today, Vol. 394, 2022, pp. 190-197, https://doi.org/10.1016/j.cattod.2021.10.012.

[3] T. D. V. Phuong, L. M. Quynh, N. N. Viet, N. T. Son, V. H. Pham, P. D. Tam, V. H. Nguyen, T. L. Manh, Effect of Temperature on the Mechanisms and Kinetics of Cobalt Electronucleation and Growth onto Glassy Carbon Electrode Using Reline Deep Eutectic Solvent, Journal of Electroanalytical Chemistry, Vol. 880, 2021, pp. 114823, https://doi.org/10.1016/j.jelechem.2020.114823.

[4] F. Soma, Q. Rayée, M. Bougouma, C. Baustert, C. B. Herman, T. Doneux, Palladium Electrochemistry in the Choline Chloride-Urea Deep Eutectic Solvent at Gold and Glassy Carbon Electrodes, Electrochimica Acta, Vol. 345, 2020, pp. 136165, https://doi.org/10.1016/j.electacta.2020.136165.

[5] Y. Choi, J. Kim, H. G. Seo, H. L. Tuller, W. Jung, Nucleation and Growth Kinetics of Electrochemically Deposited Ceria Nanostructures for High-Temperature Electrocatalysis, Electrochimica Acta, Vol. 316, 2019, pp. 273-282, https://doi.org/10.1016/j.electacta.2019.05.135.

[6] K. Gao, X. Wei, G. Liu, B. Zhang, J. Zhang, Electrodeposition and Biocompatibility of Palladium and Phosphorus Doped Amorphous Hydrogenated Carbon Films, Chemical Physics, Vol. 537, 2020, pp. 110857, https://doi.org/10.1016/j.chemphys.2020.110857.

[7] I. Danaee, 2D–3D Nucleation and Growth of Palladium on Graphite Electrode, Journal of Industrial and Engineering Chemistry, Vol. 19, 2013, pp. 1008-1013, https://doi.org/10.1016/j.jiec.2012.11.024.

[8] S. Avisar, A. Shvets, Y. Shner, I. Popov, A. Bino, Nano-Porous Ruthenium-Palladium and Ruthenium-Platinum Alloys and Their Application as Hydrogenation Catalysts, Journal of Alloys and Compounds, Vol. 936, 2023, pp. 168326, https://doi.org/10.1016/j.jallcom.2022.168326.

[9] A. F. Oliveira, S. M. Silva, C. P. Rubinger, J. Ider, R. M. Rubinger, E. T. M. Oliveira, A. C. Doriguetto, H. B. D. Carvalho, Preparation and Characterization of Palladium-doped Titanium Dioxide for Solar Cell Applications, Materials Science and Engineering: B, Vol. 280, 2022, pp. 115702, https://doi.org/10.1016/j.mseb.2022.115702.

[10] J. Liu, H. Yu, L. Wang, Z. Deng, S. Z. Vatsadze, In-situ Preparation of Palladium Nanoparticles Loaded Ferrocene Based Metal-Organic Framework and its Application in Oxidation of Benzyl Alcohol, Journal of Molecular Structure, Vol. 1198, 2019, pp. 126895, https://doi.org/10.1016/j.molstruc.2019.126895.

[11] J. Sun, Y. Li, Y. Liu, W. Zhou, X. Zhen, M. F. Lang, Facile Fabrication of a Flexible Electrode by Electrodeposition of Palladium on Silver Nanowires for Ethanol Oxidation, International Journal of Hydrogen Energy, Vol. 44, 2019, pp. 5990-5996, https://doi.org/10.1016/j.ijhydene.2019.01.138.

[12] D. Song, Y. Li, X. Lu, M. Sun, H. Liu, G. Yu, F. Gao, Palladium-Copper Nanowires-based Biosensor for the Ultrasensitive Detection of Organophosphate Pesticides, Analytica Chimica Acta, Vol. 982, 2017, pp. 168-175, https://doi.org/10.1016/j.aca.2017.06.004.

[13] P. Santhosh, K. M. Manesh, S. Uthayakumar, S. Komathi, A. I. Gopalan, K. P. Lee, Fabrication of Enzymatic Glucose Biosensor Based on Palladium Nanoparticles Dispersed onto Poly (3, 4-Ethylenedioxythiophene) Nanofibers, Bioelectrochemistry, Vol. 75, 2009, pp. 61-66, https://doi.org/10.1016/j.bioelechem.2008.12.001.

[14] H. Wang, Y. Zhang, H. Li, B. Du, H. Ma, D. Wu, Q. Wei, A Silver–Palladium Alloy Nanoparticle-based Electrochemical Biosensor for Simultaneous Detection of Ractopamine, Clenbuterol and Salbutamol, Biosensors and Bioelectronics, Vol. 49, 2013, pp. 14-19, https://doi.org/10.1016/j.bios.2013.04.041.

[15] I. Danaee, Kinetics and Mechanism of Palladium Electrodeposition on Graphite Electrode by Impedance and Noise Measurements, Journal of Electroanalytical Chemistry, Vol. 662, 2011, pp. 415-420, https://doi.org/10.1016/j.jelechem.2011.09.012.

[16] S. C. Chen, G. C. Tu, C. C. Y. Hung, C. A. Huang, M. H. Rei, Preparation of Palladium Membrane by Electroplating on AISI 316L Porous Stainless Steel Supports and its Use for Methanol Steam Reformer, Journal of Membrane Science, Vol. 314, 2008, pp. 5-14, https://doi.org/10.1016/j.memsci.2007.12.066.

[17] C. H. Lee, S. C. Wang, C. J. Yuan, M. F. Wen, K. S. Chang, Comparison of Amperometric Biosensors Fabricated by Palladium Sputtering, Palladium Electrodeposition and Nafion/Carbon Nanotube Casting on Screen-Printed Carbon Electrodes, Biosensors and Bioelectronics, Vol. 22, 2007, pp. 877-884, https://doi.org/10.1016/j.bios.2006.03.008.

[18] I. E. E. López, M. R. Romo, M. G. M. D. O. Yemha, P. M. Gil, M. T. R. Silva, J. Mostany, M. P. Pardavé, Palladium Nanoparticles Electrodeposition onto Glassy Carbon from a Deep Eutectic Solvent at 298 K and Their Catalytic Performance toward Formic Acid Oxidation, Journal of the Electrochemical Society, Vol. 166, 2018, pp. 3205-3211, https://doi.org/10.1149/2.0251901jes.

[19] K. Yoshii, Y. Oshino, N. Tachikawa, K. Toshima, Y. Katayama, Electrodeposition of Palladium from Palladium (II) Acetylacetonate in an Amide-type Ionic Liquid, Electrochemistry Communications, Vol. 52, 2015, pp. 21-24, https://doi.org/10.1016/j.elecom.2015.01.003.

[20] G. Lanzinger, R. Böck, R. Freudenberger, T. Mehner, I. Scharf, T. Lampke, Electrodeposition of Palladium Films from Ionic Liquid (IL) and Deep Eutectic Solutions (DES): Physical–Chemical Characterisation of Non-Aqueous Electrolytes and Surface Morphology of Palladium Deposits, Transactions of the IMF, Vol. 91, 2013, pp. 133-140, https://doi.org/10.1179/0020296713Z.00000000097.

[21] M. Manolova, R. Böck, Electrodeposition of Pd from a Deep Eutectic Solvent System: Effect of Additives and Hydrodynamic Conditions, Transactions of the IMF, Vol. 97, 2019, pp. 161-168, https://doi.org/10.1080/00202967.2019.1605755.

[22] D. V. P. Thao, D. T. T. Ngan, D. V. Tuan, H. Lan, N. T. Nguyet, V. V. Thu, V. P. Hung, P. D. Tam, Facile Preparation of Copper Nanoparticles in Environmentally Friendly Solvent for DNA Sensor Application, Materials Today Communications, Vol. 33, 2022, pp. 104161, https://doi.org/10.1016/j.mtcomm.2022.104161.

[23] E. L. Smith, A. P. Abbott, K. S. Ryder, Deep Eutectic Solvents (DESs) and Their Applications, Chemical Reviews, Vol. 114, 2014, pp. 11060-11082, https://doi.org/10.1021/cr300162p.

[24] A. S. Fuentes, A. F. Filippin, M. D. C. Aguirre, Pd nucleation and Growth Mechanism Deposited on Different Substrates, Procedia Materials Science, Vol. 8, 2015, pp. 541-550, https://doi.org/10.1016/j.mspro.2015.04.107.

[25] M. D. C. Aguirre, Nucleation and Growth Mechanisms of Palladium, Nanoflower-Shaped, and its Performance as Electrocatalyst in the Reduction of Cr (VI), Journal of Applied Electrochemistry, Vol. 49, 2019, pp. 795-809, https://doi.org/10.1007/s10800-019-01323-0.

[26] N. Elgrishi, B. D. M. Carthy, E. S. Rountree, J. L. Dempsey, Reaction Pathways of Hydrogen-Evolving Electrocatalysts: Electrochemical and Spectroscopic Studies of Proton-Coupled Electron Transfer Processes, ACS Catalysis, Vol. 6, 2016, pp. 3644-3659, https://doi.org/10.1021/acscatal.6b00778.

[27] J. M. Savéant, C. Costentin, Elements of Molecular and Biomolecular Electrochemistry: An Electrochemical Approach to Electron Transfer Chemistry, John Wiley & sons Inc., 2019.

[28] K. Izutsu, Electrochemistry in Nonaqueous Solutions, Wiley-VCH, 2009.

[29] M. Jafarian, F. Gobal, I. Danaee, M.G. Mahjani, Impedance Spectroscopy Study of Aluminum Electrocrystallization from Basic Molten Salt ($AlCl_3$–NaCl–KCl), Electrochimica Acta, Vol. 52, 2007, pp. 5437-5443, https://doi.org/10.1016/j.electacta.2007.02.068.

[30] A. J. Bard, L. R. Faulkner, Electrochemical Methods: Fundamental and Applications, John Wiley & Sons, Inc., 2001.

[31] M. P. Pardavé, B. R. Scharifker, E. M. Arce, M. R. Romo, Nucleation and Diffusion-Controlled Growth of Electroactive Centers: Reduction of Protons during Cobalt Electrodeposition, Electrochimica Acta, Vol. 50, 2005, pp. 4736-4745, https://doi.org/10.1016/j.electacta.2005.03.004.

[32] B. J. Hwang, R. Santhanam, Y. L. Lin, Nucleation and Growth Mechanism of Electroformation of Polypyrrole on a Heat-Treated Gold/Highly Oriented Pyrolytic Graphite, Electrochimica Acta, Vol. 46, 2001, pp. 2843-2853, http://dx.doi.org/10.1016/S0013-4686(01)00495-9.

[33] J. V. Sanchez, R. Diaz, P. Herrasti, P. Ocon, Electrogeneration and Characterization of Poly (3-Methylthiophene), Polymer Journal, Vol. 33, 2001, pp. 514-521, https://doi.org/10.1295/polymj.33.514.